

Measures of Three-Dimensional Anisotropy and Intermittency in Strong Alfvénic Turbulence

A. Mallet^{1,2*}, A. A. Schekochihin^{2,3}, B. D. G. Chandran^{1,3}, C. H. K. Chen⁴,
T. S. Horbury⁴, R. T. Wicks⁵ and C. C. Greenan⁶

¹Space Science Center, University of New Hampshire, Durham, NH 03824, USA

²Rudolf Peierls Centre for Theoretical Physics, University of Oxford, Oxford OX1 3NP, United Kingdom

³Merton College, Oxford OX1 4JD, United Kingdom

⁴Department of Physics, Imperial College London, London SW7 2AZ, United Kingdom

⁵Institute for Risk and Disaster Reduction, University College London, London, WC1E 6BT, United Kingdom

⁶Department of Statistics, University of Oxford, Oxford OX1 3TG, United Kingdom

7 December 2015

ABSTRACT

We measure the local anisotropy of numerically simulated strong Alfvénic turbulence with respect to two local, physically relevant directions: along the local mean magnetic field and along the local direction of one of the fluctuating Elsasser fields. We find significant scaling anisotropy with respect to both these directions: the fluctuations are “ribbon-like” — statistically, they are elongated along both the mean magnetic field and the fluctuating field. The latter form of anisotropy is due to scale-dependent alignment of the fluctuating fields. The intermittent scalings of the n th-order conditional structure functions in the direction perpendicular to both the local mean field and the fluctuations agree well with the theory of Chandran et al. (2015), while the parallel scalings are consistent with those implied by the critical-balance conjecture. We quantify the relationship between the perpendicular scalings and those in the fluctuation and parallel directions, and find that the scaling exponent of the perpendicular anisotropy (i.e., of the aspect ratio of the Alfvénic structures in the plane perpendicular to the mean magnetic field) depends on the amplitude of the fluctuations. This is shown to be equivalent to the anticorrelation of fluctuation amplitude and alignment at each scale. The dependence of the anisotropy on amplitude is shown to be more significant for the anisotropy between the perpendicular and fluctuation-direction scales than it is between the perpendicular and parallel scales.

Key words: MHD – turbulence – solar wind

1 INTRODUCTION

Strong plasma turbulence is present in a wide range of astrophysical systems, and is directly measured by spacecraft in the solar wind (e.g., Bruno & Carbone 2013). In the presence of a strong mean magnetic field \mathbf{B}_0 , on scales longer than the ion gyroradius, the Alfvénically polarized fluctuations decouple from the compressive fluctuations and satisfy the reduced magnetohydrodynamic (RMHD) equations. These can be derived both as an anisotropic limit of standard MHD (Strauss 1976; Kadomtsev & Pogutse 1974) and as a large-scale limit of gyrokinetics (Schekochihin et al. 2009), meaning that they describe the turbulence in both strongly and weakly collisional plasmas. Written using Elsasser (1950) variables $\mathbf{z}_\perp^\pm = \mathbf{u}_\perp \pm \mathbf{b}_\perp$, where \mathbf{u}_\perp and \mathbf{b}_\perp are the velocity and magnetic-field (in velocity units) perturbations perpendicular to

\mathbf{B}_0 , the RMHD equations are

$$\partial_t \mathbf{z}_\perp^\pm \mp v_A \partial_z \mathbf{z}_\perp^\pm + \mathbf{z}_\perp^\mp \cdot \nabla_\perp \mathbf{z}_\perp^\pm = -\nabla_\perp p, \quad (1)$$

where the pressure p is determined from $\nabla_\perp \cdot \mathbf{z}^\pm = 0$, $v_A = |\mathbf{B}_0|$ is the Alfvén speed, and we have taken \mathbf{B}_0 to be in the z direction.

The turbulence described by Eqs. (1) is known to be anisotropic with respect to the local magnetic-field direction, in both numerical simulations and in the solar wind (Cho & Vishniac 2000; Maron & Goldreich 2001; Horbury et al. 2008; Podesta et al. 2009; Wicks et al. 2010; Chen et al. 2011; Beresnyak 2015), with the anisotropy increasing at smaller scales. This anisotropy is explained by the critical-balance conjecture (Goldreich & Sridhar 1995, 1997), which posits that the nonlinear time τ_{nl}^\pm and Alfvén (linear) time $\tau_A^\pm \doteq l_\parallel^\pm / v_A$ must be comparable at each scale, where l_\parallel is the coherence length along the magnetic field lines. The dynamics of weak turbulence ($\tau_A^\pm \ll \tau_{nl}^\pm$) lead to a decrease in τ_{nl}^\pm until $\tau_A^\pm \sim \tau_{nl}^\pm$, while if $\tau_A \gg \tau_{nl}$, it is causally impossible to maintain the parallel coherence over length l_\parallel , so l_\parallel —

* Contact e-mail: alfred.mallet@unh.edu

and thus τ_A — adjust until $\tau_A^\pm \sim \tau_{nl}^\pm$ (Goldreich & Sridhar 1997; Nazarenko & Schekochihin 2011). This guarantees that the two timescales are comparable, and so the cascade time is, inevitably, $\tau_c \sim \tau_A^\pm \sim \tau_{nl}^\pm$. By an argument following Kolmogorov (1941), the scale independence of the mean energy flux,

$$\varepsilon^\pm \sim \frac{(\delta z_\perp^\pm)^2}{\tau_c} \sim \frac{(\delta z_\perp^\pm)^2 v_A}{l_\parallel^\pm} \sim \text{const}, \quad (2)$$

implies that $(\delta z_\perp^\pm)^2 \sim l_\parallel^\pm (\varepsilon^\pm / v_A)$, or, equivalently, the energy spectra of the Elsasser fields have a spectral index in the parallel direction of -2 , regardless of the details of the nonlinear term. This is seen in both measurements of the solar wind and simulations cited above.

The perpendicular scaling is harder to establish because only \mathbf{z}_\perp^\pm that has a gradient in the direction of \mathbf{z}_\perp^\mp gives rise to a nonzero contribution to the RMHD nonlinearity, $\mathbf{z}_\perp^\mp \cdot \nabla_\perp \mathbf{z}_\perp^\pm$. Combined with the fact that the Elsasser-fields are 2D-solenoidal, $\nabla_\perp \cdot \mathbf{z}_\perp^\pm = 0$, this means that *dynamic alignment* (Boldyrev 2006) of their fluctuation vectors to within a small angle θ^\pm of each other will decrease the nonlinearity by a factor $\sin \theta^\pm$. The nonlinear time may, therefore, be defined as

$$\tau_{nl}^\pm \doteq \frac{\lambda}{\delta z_\perp^\mp \sin \theta^\pm}, \quad (3)$$

where λ is the perpendicular coherence length. If θ is correlated with amplitude in a scale-dependent manner, this can alter the scaling behaviour of the nonlinear time, and, therefore, the scaling of the fluctuation amplitudes. There is continuing disagreement as to whether the numerical evidence that supports the scale-dependence of the dynamic alignment angle $\sin \theta^\pm$ is truly representative of the asymptotic state of the RMHD inertial range (Perez et al. 2014; Beresnyak 2014).

The alignment of the fields and the consequent reduction in the nonlinearity can also be linked to anisotropy within the perpendicular plane (Boldyrev 2006)¹. Critical balance implies that

$$\frac{l_\parallel}{v_A} \sim \frac{\lambda}{\delta z_\perp^\pm \sin \theta^\pm}, \quad (4)$$

where l_\parallel is now taken to be the coherence length along the magnetic field of the combination of the fluctuating fields which make up the structure, \mathbf{z}_\perp^+ and \mathbf{z}_\perp^- . Meanwhile, the distance that the magnetic field lines wander in the perpendicular plane is typically of order

$$\xi \sim \frac{\max(\delta z_\perp^+, \delta z_\perp^-)}{v_A} l_\parallel, \quad (5)$$

where we choose the maximum of the two Elsasser fields because $b_\perp \approx z_\perp^\pm/2$ when $z_\perp^\pm \gg z_\perp^\mp$. Since l_\parallel is the coherence length along the field line, the combined \mathbf{z}_\perp^+ and \mathbf{z}_\perp^- fluctuations must also be coherent *in their own direction* (the "fluctuation direction") over at least the distance ξ . This direction is defined to within an angle θ^\pm , because the fields are aligned with each other within that angle. Therefore, the typical aspect ratio of coherent structures within the

perpendicular plane is λ/ξ . Comparing Eqs. (4) and (5), we find that

$$\sin \theta^\pm \sim \frac{\lambda}{\xi} \doteq \sin \theta. \quad (6)$$

The same argument was used by Boldyrev (2006) for the angle between $\delta \mathbf{u}_\perp$ and $\delta \mathbf{b}_\perp$, θ^{ub} , instead of θ^\pm : either angle being small reduces the nonlinearity, so whichever is smaller in the sheetlike structures will generally constrain the aspect ratio λ/ξ better.

Combined with the anisotropy in the parallel direction, the above argument implies that the turbulence may exhibit 3D anisotropy in an instantaneous local basis defined by the directions of the mean magnetic field, the fluctuations, and the direction perpendicular to both. Equivalently, turbulent fluctuations may have different coherence scales l_\parallel , ξ , and λ in these three directions².

It is not hard to show that scale-dependent perpendicular anisotropy cannot exist without non-self-similar scale dependence of the joint distribution of the vector field-increments, i.e., without intermittency. Suppose the joint distribution $p(\delta \mathbf{z}_\perp^\pm | r_\perp)$ were invariant when the amplitude were rescaled by r_\perp^a , i.e., the rescaled vector variable $\mathbf{w} = \delta \mathbf{z}_\perp^\pm / r_\perp^a$ had a distribution that did not depend on r_\perp . The fact that the whole joint distribution is invariant means that not only are the amplitudes non-intermittent, but the angle

$$\theta_{\delta z_\perp^\pm} = \arctan \frac{\delta z_{\perp x}^\pm}{\delta z_{\perp y}^\pm} = \arctan \frac{w_x}{w_y} \quad (7)$$

also has a distribution independent of r_\perp . This guarantees that the conditional n th-order structure function has an angle-independent scaling:

$$S_{n,3D} = \langle (\delta z_\perp^\pm)^n | \theta_{\delta z_\perp^\pm}, r_\perp \rangle = r_\perp^{na} \langle w^n | \theta_{\delta z_\perp^\pm} \rangle = r_\perp^{na} f_n(\theta_{\delta z_\perp^\pm}), \quad (8)$$

where the unknown function f_n cannot depend on r_\perp . Thus, if the vector $\delta \mathbf{z}_\perp^\pm$ is non-intermittent (has a scale-invariant distribution), it cannot have scale-dependent perpendicular anisotropy or equivalently, according to the argument earlier in this Introduction, scale-dependent alignment.

In this paper, we study the 3D anisotropy and intermittency in numerically simulated RMHD turbulence, using a 3D conditional structure function method, described in Section 2, which was first used by Chen et al. (2012) for measurements in the solar wind. In Section 3, we present the results obtained using second-order conditional structure functions, showing that there is indeed significant 3D anisotropy. In Section 4, we go further, and present the results of the 3D conditional structure function analysis for structure functions of up to 5th order, showing that the turbulence is highly intermittent in all three directions, and comparing the scalings in the perpendicular direction to a recent theoretical model of intermittency in Alfvénic turbulence (Chandran et al. 2015), finding that the measurements are consistent with this model. The scalings in the parallel and fluctuation directions are compared to a simple model where anisotropies do not depend on amplitude at a particular scale, which turns out to be slightly inconsistent with the data. This implies that the anisotropy is itself intermittent. In Section 5, we present a quantitative analysis of this *intermittency of anisotropy*, and show that the scaling exponents of the aspect ratios λ/ξ and λ/l_\parallel increase

¹ The argument that follows only applies to sheetlike structures. Aligned circular structures are also possible (Perez & Chandran 2013), but sheets have been observed as the dominant structures in MHD turbulence in a wide range of studies (Grauer et al. 1994; Politano et al. 1995; Maron & Goldreich 2001; Greco et al. 2010). Recently, Howes (2015) has shown that the Alfvén wave dynamics lead naturally to the formation of sheetlike structures, and so our restriction to this type of structures is motivated by analysis of direct numerical simulations of the turbulence.

² One expects some degree of anisotropy within the perpendicular plane just due to kinematic constraints imposed by the solenoidality of the fields \mathbf{z}_\perp^\pm . We discuss this issue in the Appendix, showing that solenoidality does not directly constrain the conditional structure function.

with the order n of the structure functions that one uses to calculate them. We show that the perpendicular aspect ratio $\sin \theta \doteq \lambda/\xi$ (the anisotropy within the perpendicular plane) is significantly intermittent, while the parallel aspect ratio $\sin \phi \doteq \lambda/l_{\parallel}$ is less so. We then discuss what implications this has for the physics of the collisions of balanced Alfvénic fluctuations in the model of Chandran et al. (2015). In Section 6, we compare our results on the intermittency of the anisotropy within the perpendicular plane to the scaling of the alignment angle defined more traditionally in terms of the ratio of different structure functions (Mason et al. 2006), and conclude that they are consistent with each other, which suggests that the two methods are indeed measuring the same phenomenon. In Section 7, we summarise our conclusions and discuss the relationship between this and previous work.

2 NUMERICAL SETUP AND 3D CONDITIONAL STRUCTURE FUNCTIONS

Eqs. (1) were solved in a triply periodic box of resolution 1024^3 , using the code described in Chen et al. (2011). In the code units, $v_A = 1$ and the box has length 2π in each direction. The RMHD equations are invariant under the simultaneous rescaling

$$z \rightarrow az, v_A \rightarrow av_A \quad (9)$$

for arbitrary a . Therefore, while in code units $z_{\perp}^{\pm} \sim v_A$ and the box is cubic, in fact, when translated into physical units, the box is much longer in the parallel direction and the fluctuation amplitudes are much smaller than v_A , even as the linear and nonlinear terms remain comparable. Energy was injected via white-noise forcing at $k_{\perp} = 1, 2$ and $k_{\parallel} = 1$ and dissipated by perpendicular hyperviscosity ($\nu_{\perp} \nabla_{\perp}^8$ with $\nu_{\perp} = 2 \times 10^{-17}$). There is also an effective Laplacian parallel viscosity $\nu_{\parallel} = 1.5 \times 10^{-4}$ because the linear term is upwinded slightly; ν_{\parallel} is chosen to be small enough so that it only dissipates a small fraction ($\approx 7\%$) of the total power. The mean injected power was taken to be $\varepsilon^{\pm} = 1$, meaning that the turbulence is balanced and strong. The forcing term is purely in the velocity, and the magnetic field was not forced so as not to break the magnetic-flux conservation at the forcing scales.

We define the Elsasser-field increments as

$$\delta \mathbf{z}_{\perp}^{\pm} = \mathbf{z}_{\perp}^{\pm}(\mathbf{r}_0 + \mathbf{r}) - \mathbf{z}_{\perp}^{\pm}(\mathbf{r}_0), \quad (10)$$

where \mathbf{r}_0 is an arbitrary point (arbitrary because we consider homogeneous turbulence), and \mathbf{r} is the separation vector, with length r and direction $\hat{\mathbf{r}} = \mathbf{r}/r$. The amplitude of the field increment in Eq. (10) is $|\delta \mathbf{z}_{\perp}^{\pm}| = |\delta \mathbf{z}_{\perp}^{\pm}|$, and its direction is $\delta \hat{\mathbf{z}}_{\perp}^{\pm} = \delta \mathbf{z}_{\perp}^{\pm}/|\delta \mathbf{z}_{\perp}^{\pm}|$. The local mean magnetic field \mathbf{B}_{loc} between \mathbf{r}_0 and $\mathbf{r}_0 + \mathbf{r}$ is defined as

$$\mathbf{B}_{\text{loc}} = \mathbf{B}_0 + \frac{1}{2} [\mathbf{b}_{\perp}(\mathbf{r}_0) + \mathbf{b}_{\perp}(\mathbf{r}_0 + \mathbf{r})], \quad (11)$$

and its direction is $\hat{\mathbf{B}}_{\text{loc}} = \mathbf{B}_{\text{loc}}/|\mathbf{B}_{\text{loc}}|$. The components of the field increment and the separation vector in the plane normal to \mathbf{B}_{loc} are

$$\begin{aligned} \delta \mathbf{z}_{\perp, N}^{\pm} &= \delta \mathbf{z}_{\perp}^{\pm} - [\delta \mathbf{z}_{\perp}^{\pm} \cdot \hat{\mathbf{B}}_{\text{loc}}] \hat{\mathbf{B}}_{\text{loc}}, \\ \mathbf{r}_{\perp} &= \mathbf{r} - [\mathbf{r} \cdot \hat{\mathbf{B}}_{\text{loc}}] \hat{\mathbf{B}}_{\text{loc}}, \end{aligned} \quad (12)$$

and the directions of these vectors are $\delta \hat{\mathbf{z}}_{\perp, N}^{\pm} = \delta \mathbf{z}_{\perp, N}^{\pm}/|\delta \mathbf{z}_{\perp, N}^{\pm}|$ and $\hat{\mathbf{r}}_{\perp} = \mathbf{r}_{\perp}/|\mathbf{r}_{\perp}|$.

The angle between \mathbf{r} and the local mean field is defined via

$$\cos \theta_{B_{\text{loc}}} = \hat{\mathbf{r}} \cdot \hat{\mathbf{B}}_{\text{loc}}. \quad (13)$$

It is important to point out that this angle is not invariant to the

rescaling in Eq. (9), and so, to compare the dependence of the structure functions (Figure 1(b)) on this angle to a situation with a given aspect ratio (or fluctuation level), one must rescale it assuming some specific aspect ratio a [see Eq. (9)] of the physical box, rather than the nominal value of 1 used in RMHD simulations. However, $\theta_{B_{\text{loc}}} = 0^\circ, 90^\circ$ are fixed points under any such rescaling. The angle between \mathbf{r}_{\perp} and the perpendicular fluctuation $\delta \mathbf{z}_{\perp}^{\pm}$ is defined via

$$\cos \theta_{\delta z_{\perp}^{\pm}} = \hat{\mathbf{r}}_{\perp} \cdot \delta \hat{\mathbf{z}}_{\perp, N}^{\pm}. \quad (14)$$

If $\theta_{B_{\text{loc}}} = 90^\circ$ and $\theta_{\delta z_{\perp}^{\pm}} = 0^\circ$, then the point separation \mathbf{r} is along the "fluctuation direction", while if $\theta_{B_{\text{loc}}} = 90^\circ$ and $\theta_{\delta z_{\perp}^{\pm}} = 90^\circ$, it is along the direction perpendicular to both the fluctuation and the local mean field, which we will call the "perpendicular direction". If $\theta_{B_{\text{loc}}} = 0^\circ$, the separation is along the "parallel direction". The angles $\theta_{B_{\text{loc}}}$ and $\theta_{\delta z_{\perp}^{\pm}}$, along with the point separation r , define a locally-varying coordinate system referred to the two directions that we expect to be physically important³.

The n th-order conditional structure function of \mathbf{z}_{\perp}^{\pm} at point separation r and the pair of angles $\theta_{B_{\text{loc}}}, \theta_{\delta z_{\perp}^{\pm}}$,

$$S_{n, 3D}(\theta_{B_{\text{loc}}}, \theta_{\delta z_{\perp}^{\pm}}, r) = \langle (\delta z_{\perp}^{\pm})^n | \theta_{B_{\text{loc}}}, \theta_{\delta z_{\perp}^{\pm}}, r \rangle, \quad (15)$$

is defined as the average of $(\delta z_{\perp}^{\pm})^n$ at the scale r , with the separation vector characterized by angles $\theta_{B_{\text{loc}}}$ and $\theta_{\delta z_{\perp}^{\pm}}$. These objects (with $n = 2$) have been used by Chen et al. (2012) for analysis of the real solar wind turbulence. The conditional structure function defines the scaling of the fluctuations at all angles to the physically distinct directions identified above, and provides a natural way to study the anisotropy in all directions using the same mathematical object. Our subsequent analysis is based on the calculation of these structure functions using data from the numerical simulation described above.

To achieve this, snapshots of the fields in the simulation were taken at 10 different times separated by more than a turnover time, viz., every 2 code time units. For each of the snapshots, 8×10^6 pairs of points $\mathbf{r}_0, \mathbf{r}_0 + \mathbf{r}$ were chosen at each of 32 different logarithmically spaced separation scales r . The direction $\hat{\mathbf{r}}$ was uniformly distributed over a sphere. For each pair of points, the Elsasser-field increment amplitudes δz_{\perp}^{\pm} and the three angles $\theta_{B_{\text{loc}}}, \theta_{\delta z_{\perp}^{\pm}}$ were recorded. All angles were collapsed onto the interval $[0^\circ, 90^\circ]$. The structure-function values reported here are the means over all 10 snapshots, and the error bars show the standard deviation from the means calculated for each snapshot.

To calculate the n -th order conditional structure functions in Eq. (15), we bin the field-increment amplitudes δz_{\perp}^{\pm} by the pair of angles $\theta_{B_{\text{loc}}}, \theta_{\delta z_{\perp}^{\pm}}$. Here we will only show the structure functions of δz_{\perp}^{\pm} ; the δz_{\perp}^{\mp} structure functions are the same because the turbulence is balanced. The conditional average in Eq. (15) was calculated over an angle bin $10(i-1)^\circ \leq \theta_{B_{\text{loc}}} < 10i^\circ$, $10(j-1)^\circ \leq \theta_{\delta z_{\perp}^{\pm}} < 10j^\circ$, where i and j range from 1 to 9. Some special cases of this structure function deserve particular at-

³ It is important to distinguish between the many angles (and aspect ratios) defined in this paper: $\theta^{\pm}, \theta^{ub}$ are the angles between field increments, $\sin \theta$ is the aspect ratio of structures in the local basis, and $\theta_{B_{\text{loc}}}, \theta_{\delta z_{\perp}^{\pm}}$ are angles describing the relative arrangement of fields and separation vectors \mathbf{r} . They are not necessarily the same, although we have argued that θ is determined by the smaller of θ^{\pm} and θ^{ub} .

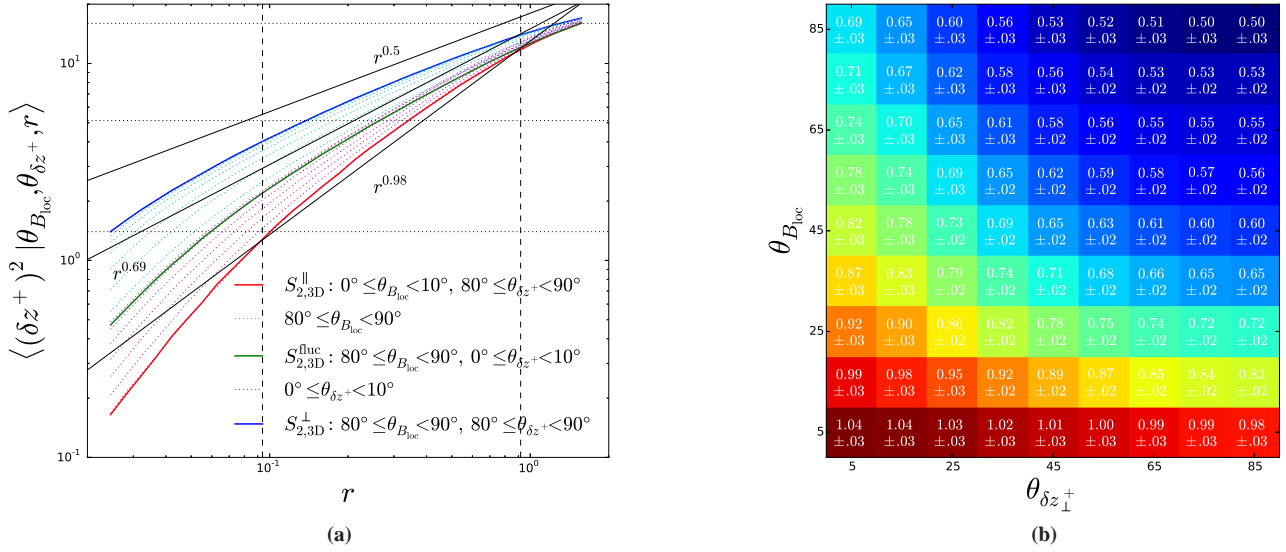


Figure 1. (a) The conditional second-order structure functions [Eq. (15)] plotted for different angle intervals. In dark blue (solid line) is the structure function $S_{2,3D}^{\perp}$ in the angle bin most perpendicular to both the local mean magnetic field and the $\delta \mathbf{z}_{\perp}^+$ fluctuations, in green (solid line), the structure function $S_{2,3D}^{\text{fluc}}$ in the angle bin closest to the direction $\delta \mathbf{z}_{\perp}^+$, and in red (solid line), the structure function $S_{2,3D}^{\parallel}$ in the angle bin closest to the parallel direction $\hat{\mathbf{B}}_{loc}$. In cyan (dotted lines), are the structure functions in the whole range of $\theta_{\delta z^+}$ bins, with the angle to the mean field $80^\circ \leq \theta_{B_{loc}} < 90^\circ$, and in magenta (dotted lines), the structure functions in the whole range of $\theta_{B_{loc}}$ bins, but with the angle to the fluctuation $0^\circ \leq \theta_{\delta z^+} \leq 10^\circ$ bin. The dotted horizontal lines show the values of the structure function for which the “statistical eddies” in Figure 2 were calculated, while the vertical dashed lines show the range over which the structure-function scaling exponents were measured. **(b)** The second-order structure function exponents $\zeta_2(\theta_{B_{loc}}, \theta_{\delta z^+})$ and the associated errors, in all angle bins. It should be noted that to compare directly with a real situation (e.g., the solar wind), the angle $\theta_{B_{loc}}$ must be rescaled assuming a specific physical aspect ratio of the simulation box rather than the nominal aspect ratio of 1 [see Eq. (9)].

tention and particular notation:

$$\begin{aligned}
 i = 1 : & \quad S_{n,3D}^{\parallel}, \quad \text{“parallel” structure function,} \\
 i = 9, j = 1 : & \quad S_{n,3D}^{\text{fluc}}, \quad \text{“fluctuation-direction” structure function,} \\
 i = 9, j = 9 : & \quad S_{n,3D}^{\perp}, \quad \text{“perpendicular” structure function.}
 \end{aligned}$$

These bins correspond to fluctuations aligned most closely with the physical directions $\hat{\mathbf{B}}_{loc}$ (parallel), $\delta \mathbf{z}_{\perp}^+$ (fluctuation), and $\hat{\mathbf{B}}_{loc} \times \delta \mathbf{z}_{\perp}^+$ (perpendicular). We will refer to the scales at which those particular structure functions are sampled as the parallel scale l_{\parallel} , fluctuation-direction scale ξ , and perpendicular scale λ , respectively.

3 SECOND-ORDER CONDITIONAL STRUCTURE FUNCTIONS

Figure 1 shows the conditional second-order structure functions at different angles $\theta_{B_{loc}}$ and $\theta_{\delta z^+}$. These structure functions were fit to power laws over the inertial range, defined here as $0.09 < r < 0.92$. We define $\zeta_n(\theta_{B_{loc}}, \theta_{\delta z^+})$ as the scaling exponent of the n th-order structure function at that pair of angles, viz.,

$$S_{n,3D}(\theta_{B_{loc}}, \theta_{\delta z^+}) \propto r^{\zeta_n(\theta_{B_{loc}}, \theta_{\delta z^+})}. \quad (16)$$

Furthermore, we define ζ_n^{\parallel} , ζ_n^{fluc} and ζ_n^{\perp} as the scaling exponents for the parallel, fluctuation-direction, and perpendicular structure functions respectively, as defined in the previous section. The scalings for the second-order structure functions were

$$\zeta_2^{\perp} = 0.50 \pm 0.03, \quad \zeta_2^{\text{fluc}} = 0.69 \pm 0.03, \quad \zeta_2^{\parallel} = 0.98 \pm 0.03,$$

where the errors indicate standard deviations from the mean exponent obtained using the 10 snapshots. Thus, the turbulence exhibits significant scaling anisotropy (i.e., different scalings) with respect to all three directions identified here. The exponent in the parallel direction is very close to 1, in good agreement with the critical-balance scaling from Eq. (2). Thus, the parallel scaling ζ_2^{\parallel} is consistent with the critical-balance conjecture. The difference between ζ_2^{\perp} and ζ_2^{fluc} is consistent with the idea that the turbulent fluctuations become progressively more aligned as they cascade to smaller scales (cf. Boldyrev 2006, who predicts $\zeta_2^{\perp} = 1/2$ and $\zeta_2^{\text{fluc}} = 2/3$).

Based on surfaces of constant second-order structure function [Eq. (15)], one can visualize a “statistical eddy”, showing the 3D structure of turbulent correlations, in the same manner as was done for solar-wind data by Chen et al. (2012). This is done in Figure 2 for structure-function values corresponding to the outer scale, midway through the inertial range, and near the bottom of the inertial range. Statistically, due to the isotropic forcing, the structures at large scales are isotropic with respect to the local basis⁴, but become increasingly “pancake”-, or “ribbon”-like deeper in the inertial range.

One might expect some level of anisotropy imposed by constraints due to the solenoidality of the Elsasser fields. This issue

⁴ Note that the parallel and perpendicular correlation lengths appear similar only because we use the nominal box aspect ratio 1. This can be arbitrarily rescaled in RMHD [see Eq. (9)].

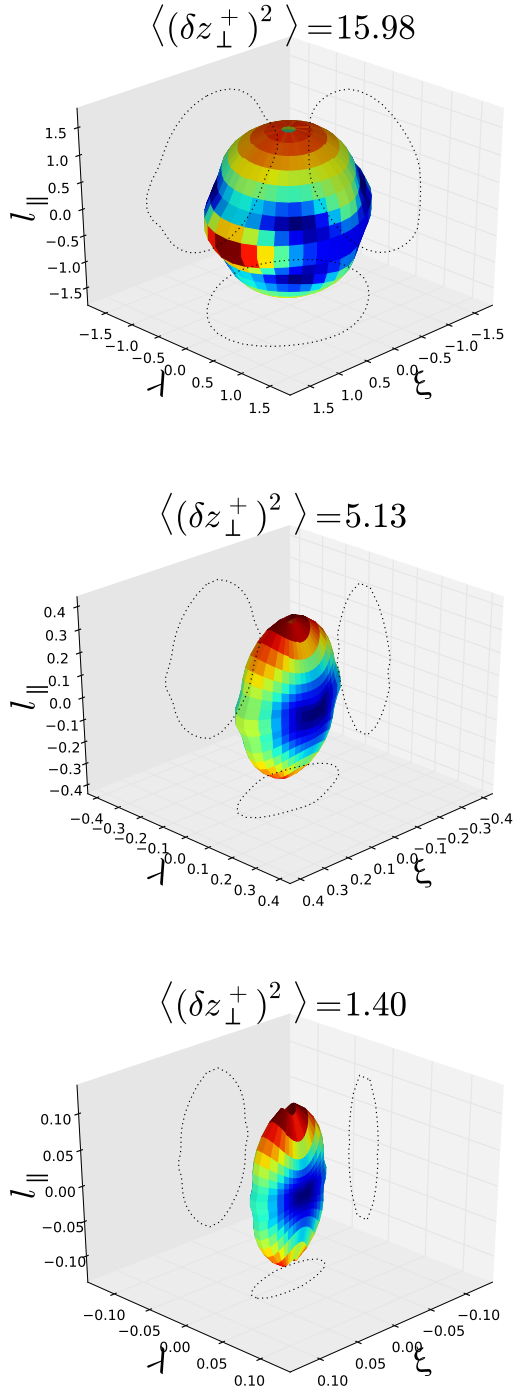


Figure 2. From top to bottom, “statistical eddies” (surfaces of constant second-order structure function) at structure function values corresponding to the outer scale, roughly halfway down the inertial range, and at the bottom of the inertial range, respectively. These values are shown as three horizontal dotted lines in Figure 1(a).

is discussed in the Appendix, where we find that the solenoidality does not directly constrain the conditional structure function.

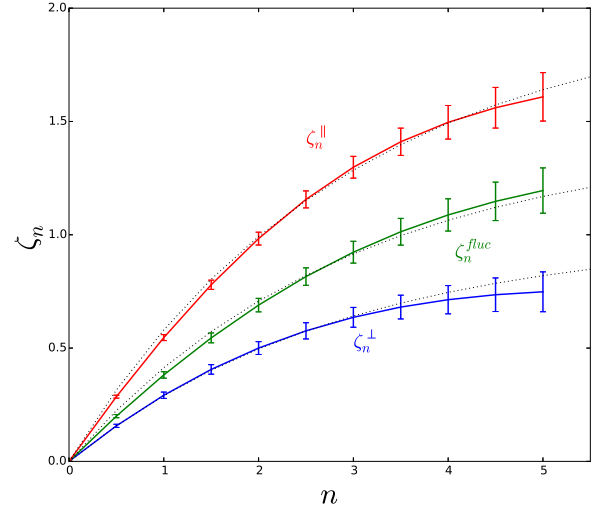


Figure 3. The exponents of conditional n th-order structure functions [Eq. (15)] in the perpendicular (blue), fluctuation (green) and parallel (red) directions, ζ_n^{\perp} , ζ_n^{fluc} and ζ_n^{\parallel} respectively. The lowest black dotted line is Eq. (18) with $\beta = 0.71$, and the middle and highest black dotted lines are that equation with the same β , divided by $\gamma = 0.69$ and $\alpha = 0.49$, respectively.

4 3D INTERMITTENCY

As we showed in the Introduction, to exhibit scaling anisotropy within the local perpendicular plane as seen in Section 3, Elsasser fields must have non-self-similar scale-dependent probability distribution functions. In this section, we study the scale dependence of the distribution functions of the field increments: the intermittency of the conditional structure functions, as a function of the two local angles $\theta_{B_{\text{loc}}}$ and $\theta_{\delta z^+}$. One common measure of intermittency is the nonlinear dependence on n of the exponents of the n th order structure functions. We extend this approach by measuring ζ_n^{\parallel} , ζ_n^{fluc} and ζ_n^{\perp} — the exponents of the parallel, fluctuation-direction, and perpendicular conditional structure functions defined in Section 2. These exponents are shown in Figure 3 up to $n = 5$. An immediate conclusion is that not only is RMHD turbulence intermittent, but it is perhaps differently intermittent in all three directions. We will study these scalings in more detail in this section.

Recently, a new model of the intermittency of Alfvénic turbulence has been proposed by Chandran et al. (2015). The model involves two archetypal nonlinear interactions. Firstly, occasional *balanced collisions* between structures of similar amplitudes $\delta z_{\perp}^+ \sim \delta z_{\perp}^-$ reduce the field amplitudes. This motivates assuming a log-Poisson distribution for δz_{\perp}^{\pm} . Secondly, in *imbalanced collisions* with $\delta z_{\perp}^+ \gg \delta z_{\perp}^-$, the amplitudes of the fluctuations remain constant while the lower-amplitude field is sheared into alignment and its perpendicular scale λ reduced. The model incorporates critical balance and dynamic alignment, and predicts that the perpendicular structure function exponents are

$$\zeta_n^{\perp} = 1 - \beta^n, \quad (18)$$

where $\beta \approx 0.691$ is derived via a number of assumptions. Let us fit our perpendicular exponents to this formula, and determine β from

the fit. The best-fit value⁵ is

$$\beta = 0.71^{+0.01}_{-0.02}, \quad (19)$$

which is in remarkably good agreement with the Chandran et al. (2015) model.

It is clear from Figure 3 that the turbulence is also highly intermittent in the fluctuation (green curve) and parallel (red curve) directions. A natural question is how the parallel and fluctuation-direction scalings are related to the perpendicular ones. Chandran et al. (2015) make no prediction for ζ_n^{\parallel} or ζ_n^{fluc} . Suppose that, in some detailed sense, the parallel and fluctuation-direction coherence scales l_{\parallel} and ξ of each turbulent fluctuation themselves have power-law dependence on the perpendicular scale λ of that fluctuation, viz.,

$$l_{\parallel} \sim \lambda^{\alpha}, \quad \xi \sim \lambda^{\gamma}. \quad (20)$$

In our terminology, this is equivalent to stating that the degree of anisotropy between the parallel and perpendicular or fluctuation and perpendicular directions is not itself intermittent, meaning that the scaling of the aspect ratios

$$\sin \phi = \frac{\lambda}{l_{\parallel}} \propto \lambda^{1-\alpha}, \quad \sin \theta = \frac{\lambda}{\xi} \propto \lambda^{1-\gamma}, \quad (21)$$

is independent of the amplitude of the fluctuations. This is the same as conjecturing the following relationships between the scaling exponents of structure functions in different directions:

$$\zeta_n^{\parallel} = \frac{\zeta_n^{\perp}}{\alpha}, \quad \zeta_n^{\text{fluc}} = \frac{\zeta_n^{\perp}}{\gamma}. \quad (22)$$

From the measured scaling exponents in Figure 3, we find that the best-fit values are

$$\alpha = 0.49, \quad \gamma = 0.69. \quad (23)$$

The resulting "model" curves in Eq. (22) are also plotted on Figure 3, with Eq. (18) used for ζ_n^{\perp} . While the curves in Eq. (22) are relatively close to the measured scalings, the quality of the fits is worse than in the perpendicular direction — the model curves are not within the error bars for every n measured, for any values of α or γ . This implies that the characteristic aspect ratios in Eq. (21) have scalings that depend on the amplitude of the fluctuations, if perhaps only slightly. In the next section, we quantify this dependence and argue that it makes physical sense.

5 INTERMITTENCY OF ANISOTROPY

The dependence of the scaling of the aspect ratios in Eq. (21) on the amplitude of the fluctuations is a symptom of *intermittency of anisotropy*: the anisotropy cannot simply be rescaled in a uniform way because fluctuations with different amplitudes at the same scale will have different typical aspect ratios. If we accept that perpendicular anisotropy is related to alignment as argued in the Introduction [Eq. (6)], this is consistent with the physical model of the nonlinear interactions by Chandran et al. (2015), according to which, in an imbalanced collision, the \mathbf{z}_{\perp}^{+} and \mathbf{z}_{\perp}^{-} fields align to within an angle inversely proportional to the amplitude of the

⁵ Based on minimizing the sum of the squared residuals weighted by the standard deviation of the measurements at each order (Aitken 1936). The errors are evaluated by varying β until the curve given by Eq. (18) fails to fall completely within the error bars of the measurements of the individual exponents.

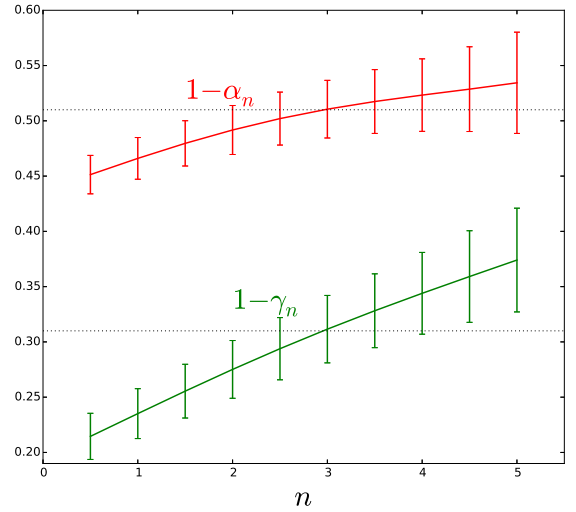


Figure 4. The aspect ratio scaling exponents $1 - \alpha_n$ (red, solid line) and $1 - \gamma_n$ (green, solid line) as a function of n [Eq. (26)]. Error bars show the standard deviation of the mean calculated from the ten snapshots. Plotted in dotted black lines are constants $1 - \alpha = 0.51$ and $1 - \gamma = 0.31$, defined in Eq. (22) and used for the dotted curves in Figure 3.

higher-amplitude fluctuation. This is also consistent with the finding of Mallet et al. (2015) that the alignment angle between $\delta \mathbf{z}_{\perp}^{+}$ and $\delta \mathbf{z}_{\perp}^{-}$ is anticorrelated with the amplitude at each scale. In fact, recalling that Mallet et al. (2015) found the critical-balance parameter

$$\chi^{\pm} \doteq \frac{\tau_A}{\tau_{nl}} \doteq \frac{l_{\parallel}^{\pm} \delta z_{\perp}^{\mp} \sin \theta^{\pm}}{v_A \lambda} \sim \frac{\delta z_{\perp}^{\mp} \sin \theta}{v_A \sin \phi} \quad (24)$$

to have a very precisely scale-invariant distribution, we realise that the simple model in Eqs. (20-21) cannot be strictly correct: since we know that δz_{\perp}^{\mp} is intermittent (non-scale-invariant), at least one of $\sin \theta$ and $\sin \phi$ must also be intermittent for the distribution of χ^{\pm} to be scale-invariant.

We quantify the intermittency of the anisotropy by generalising Eq. (22) to

$$\zeta_n^{\parallel} = \frac{\zeta_n^{\perp}}{\alpha_n}, \quad \zeta_n^{\text{fluc}} = \frac{\zeta_n^{\perp}}{\gamma_n}. \quad (25)$$

Then the aspect-ratio scalings inferred from the n th-order conditional structure function scalings using the equation above are given by

$$\sin \phi_n \propto \lambda^{1-\alpha_n}, \quad \sin \theta_n \propto \lambda^{1-\gamma_n}, \quad (26)$$

so we are now allowing some amplitude dependence of these scalings. Figure 4 shows these scalings as a function of n . Both $\sin \phi_n$ and $\sin \theta_n$ have scaling exponents that increase with n , meaning that the fluctuation amplitude and $\sin \theta$ (and, therefore, fluctuation amplitude and the alignment angle as measured by, for example, $\sin \theta^{\pm}$) are anticorrelated at each scale, confirming the result of Mallet et al. (2015) and the expectation based on the physical picture of nonlinear interactions in the model of Chandran et al. (2015). From the range of variation exhibited by α_n and γ_n in Figure 4, we conclude that the parallel aspect ratio $\sin \phi_n$ exhibits only slight intermittency, while the perpendicular aspect ratio $\sin \theta_n$ is more significantly intermittent. Note, however, that the slight variation of $1 - \alpha_n$ with n is nevertheless likely to be real: Mallet et al. (2015) found that the nonlinear time alone [Eq. (3)] was not as precisely scale-invariant as χ^{\pm} [Eq. (24)].

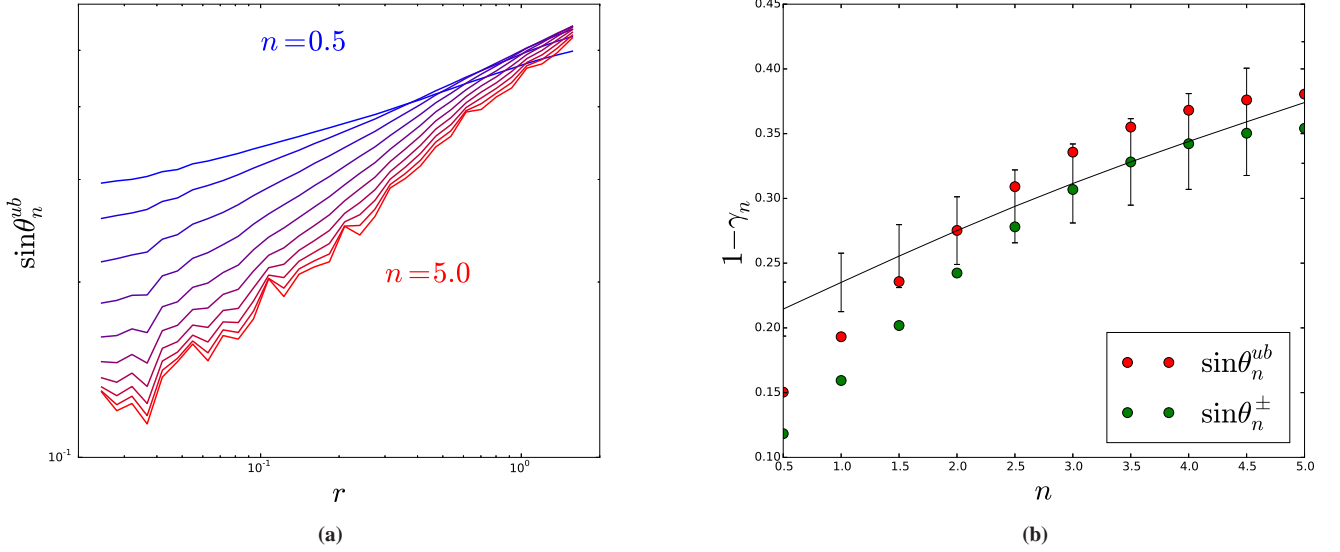


Figure 5. (a) The alignment measures $\sin \theta_n^{ub}$ [Eq. (27)] are plotted, going from $n = 0.5$ (blue) to $n = 5$ (red). (b) Comparison between the scaling exponents of $\sin \theta_n^{ub}$ (red points), the scaling exponents of $\sin \theta_n^{\pm}$ (green points) and the perpendicular alignment exponents ($1 - \gamma_n$) defined in Eq. (26) (and plotted in Figure 4).

6 COMPARISON BETWEEN DIFFERENT MEASURES OF ALIGNMENT

Had γ_n been independent of n (i.e., had the perpendicular aspect ratio $\sin \theta_n$ been non-intermittent), the alignment within the sheet-like structures would also have been non-intermittent, and it would not have mattered what method one used to measure the scaling of the alignment angle. But γ_n is intermittent, and so the precise measure of alignment does matter. Mason et al. (2006) calculated θ_n^{ub} defined by

$$\sin^n \theta_n^{ub} \equiv \frac{|\delta \mathbf{u}_{\perp} \times \delta \mathbf{b}_{\perp}|^n}{|\delta \mathbf{u}_{\perp}|^n |\delta \mathbf{b}_{\perp}|^n}, \quad (27)$$

with $n = 1$, and found that $\theta_1^{ub} \sim \lambda^{0.25}$, which they interpreted as vindication of the Boldyrev (2006) phenomenological theory (which was not concerned with intermittency). In contrast, Beresnyak & Lazarian (2006) measured

$$\sin \tilde{\theta} = \left\langle \frac{|\delta \mathbf{z}_{\perp}^+ \times \delta \mathbf{z}_{\perp}^-|}{|\delta \mathbf{z}_{\perp}^+| |\delta \mathbf{z}_{\perp}^-|} \right\rangle, \quad (28)$$

and found that this quantity exhibited virtually no scale dependence, showing that how one weights the angle by the amplitude of the fluctuation matters a great deal. We may also define another set of measures of alignment, via

$$\sin^n \theta_n^{\pm} \equiv \frac{|\delta \mathbf{z}_{\perp}^+ \times \delta \mathbf{z}_{\perp}^-|^n}{|\delta \mathbf{z}_{\perp}^+|^n |\delta \mathbf{z}_{\perp}^-|^n}. \quad (29)$$

Figure 5 shows the scale dependence of $\sin \theta_n^{ub}$ for $0.5 \leq n \leq 5$. The fact that the scaling of these alignment measures depends on how one weights them with amplitude is consistent with the idea that the alignment angle and amplitude are anticorrelated at each scale. In the foregoing, we calculated $\sin \theta_n \propto \lambda^{(1-\gamma_n)}$ in terms of the scalings of the 3D conditional structure function, and argued that $\theta_n \sim \theta_n^{ub} \sim \theta_n^{\pm}$. In Figure 5, the scaling exponents of $\sin \theta_n^{ub}$ and $\sin \theta_n^{\pm}$ are compared with $1 - \gamma_n$, where γ_n are the perpendicular alignment exponents defined in Eq. (26) and plotted

in Figure 4. The agreement is not perfect, but the three different measures show the same trend, and agree at high n , suggesting, as we argued in the Introduction, that the same physical phenomenon is being measured using our technique as in previous work.

7 DISCUSSION

The results presented in this paper show that strong Alfvénic turbulence scales highly anisotropically with respect to all three physically relevant directions: parallel ($\hat{\mathbf{B}}_{loc}$), fluctuation ($\delta \mathbf{z}_{\perp}^{\pm}$), and perpendicular ($\delta \mathbf{z}_{\perp}^{\pm} \times \hat{\mathbf{B}}_{loc}$). This anisotropy can be explained using two key physical ideas. The critical-balance conjecture underpins the parallel anisotropy, while the anisotropy within the perpendicular plane can be linked with scale-dependent alignment of the fluctuations.

The intermittent scalings ζ_n^{\perp} , ζ_n^{fluc} , ζ_n^{\parallel} of the conditional structure functions in these three directions reported here shed further light on the physics of critical balance and alignment. The perpendicular scalings agree closely with the predictions of the model of Chandran et al. (2015). The aspect-ratio scaling $\sin \theta_n = \lambda/\xi \propto \lambda^{1-\gamma_n}$ can be inferred from the ratio of the scaling exponents of the perpendicular- and fluctuation-direction structure functions, $\gamma_n = \zeta_n^{\perp}/\zeta_n^{\text{fluc}}$, and we find that the scaling exponent $1 - \gamma_n$ is an increasing function of n . This implies that the alignment angle is anticorrelated with amplitude at each scale, i.e., the alignment angle is intermittent (not scale-invariant). This promotes the view that alignment is set by mutual shearing of the Elsasser fields, which naturally leads to such anticorrelation (Chandran et al. 2015). Meanwhile, the scaling of the aspect ratio between the perpendicular and parallel directions, $\sin \phi_n \propto \lambda^{1-\alpha_n}$ varies only slightly with n (although the results of Mallet et al. (2015) suggest that this variation is real).

In the solar wind, Chen et al. (2012) applied the 3D conditional structure function technique and found essentially scale-independent anisotropy between the perpendicular and fluctuation

directions in fast solar wind. Wicks et al. (2013) also found essentially no scaling of the alignment angle in the inertial range of the fast solar wind. Chandran et al. (2015) provide a review of various different solar-wind measurements, showing that there appears to be a significant spread in the measured structure-function exponents, possibly depending on whether the measurement was from the fast or slow solar wind. This could also affect the measurement of the alignment. The difference between the fast-solar-wind measurements in Wicks et al. (2013); Chen et al. (2012) and our simulations appears to be the presence of significant anisotropy within the perpendicular plane (or equivalently, alignment) at the outer scale in the solar wind, but not in our simulations. This difference is also evident in Verdini & Grappin (2015), who link differences in the anisotropy of conditional structure functions to the expansion of the solar wind. The effect of this expansion can clearly be seen at the outer scale of their expanding box simulation, i.e. at scales where the dynamics of the cascade have not yet affected the anisotropy, but at the smaller scales anisotropy similar to that measured here is observed. Finally, Osman et al. (2014) have previously considered the intermittency of the parallel structure functions in the solar wind using the conditional structure function method, but obtained different results to those presented here. The reason for this difference requires further investigation.

Further measurements of the anisotropy and intermittency in the solar wind and of the dependence of the intermittent scalings in all directions on the solar-wind conditions would allow for new comparisons between the real turbulence and the numerical simulations presented here, and improve our understanding of the physical processes underlying dynamic alignment, critical balance, and intermittency. What appears to be suggested by the detailed study undertaken here is that all of these phenomena are very much intertwined.

ACKNOWLEDGEMENTS

This work was supported in part by NASA grant NNX15AI80G and NSF grant PHY-1500041. Simulations reported here used XSEDE, which is supported by the US NSF Grant ACI-1053575. We acknowledge support provided to ISSI/ISSI-BJ Team 304. C. H. K. Chen is supported by an Imperial College Junior Research Fellowship.

APPENDIX A: SOLENOIDALITY AND PERPENDICULAR ANISOTROPY

Since the Elsasser fields are 2D solenoidal, $\nabla_{\perp} \cdot \mathbf{z}_{\perp}^{\pm} = 0$, one might expect some degree of anisotropy with respect to the fluctuation direction within the perpendicular plane due to just this kinematic property. In this Appendix, we will outline the constraints that solenoidality places on the turbulence and to what extent this is related to anisotropic scalings of the conditional structure functions, Eq. (15).

We work within the perpendicular plane. We will use a basis for each separation \mathbf{r}_{\perp} where the x direction points along \mathbf{r}_{\perp} and the y direction is transverse to it. Since \mathbf{z}_{\perp}^{\pm} are globally isotropic (within the (x, y) plane perpendicular to the global mean magnetic field), the n th-order two-point structure function of $\delta \mathbf{z}_{\perp}^{\pm}$, the rank- n tensor $\langle \delta z_{\perp,i}^{\pm} \delta z_{\perp,j}^{\pm} \delta z_{\perp,k}^{\pm} \dots \rangle$, can be expressed as a sum of terms, each with n vector indices and composed of products of Kronecker deltas δ_{ij} and unit vectors $\hat{r}_{\perp,i}$, all with distinct indices. Moreover,

the structure function must be of such a form that it is invariant under interchange of indices. For example, the tensor second-order structure function is

$$\langle \delta z_{\perp,i}^{\pm} \delta z_{\perp,j}^{\pm} \rangle = S_{2,T}(r_{\perp})(\delta_{ij} - \hat{r}_{\perp,i} \hat{r}_{\perp,j}) + S_{2,L}(r_{\perp}) \hat{r}_{\perp,i} \hat{r}_{\perp,j}, \quad (\text{A1})$$

where $r_{\perp} = |\mathbf{r}_{\perp}|$ and the longitudinal $S_{2,L}$ and transverse $S_{2,T}$ scalar structure functions are

$$S_{2,L} = \langle (\delta \mathbf{z}_{\perp}^{\pm} \cdot \hat{\mathbf{r}}_{\perp})^2 \rangle, \quad S_{2,T} = \langle (\delta \mathbf{z}_{\perp}^{\pm} \times \hat{\mathbf{r}}_{\perp})^2 \rangle. \quad (\text{A2})$$

The solenoidality constraint is imposed by taking the divergence $\partial/\partial r_i$ of Eq. (A1) and setting it equal to zero. This gives the von Kármán relation in 2D (Batchelor 1953):

$$\frac{\partial}{\partial r_{\perp}} (r_{\perp} S_{2,L}) = S_{2,T}. \quad (\text{A3})$$

This means that in the inertial range, where $S_{2,L}$ and $S_{2,T}$ are power laws, they must scale in the same way $\propto r_{\perp}^{2a}$, and have a certain ratio $(2a + 1)$ between them:

$$S_{2,T} = D r_{\perp}^{2a}, \quad S_{2,L} = \frac{D}{2a + 1} r_{\perp}^{2a}, \quad (\text{A4})$$

where D is a constant. Thus there is a scale-independent level of "kinematic" anisotropy between the transverse and longitudinal structure functions.

The third order tensor structure function again depends on two scalar functions of r_{\perp} , each multiplying one of the only two possible rank-3 tensors, $\hat{r}_{\perp,i} \hat{r}_{\perp,j} \hat{r}_{\perp,k}$ and $\delta_{ij} \hat{r}_{\perp,k} + \delta_{jk} \hat{r}_{\perp,i} + \delta_{ki} \hat{r}_{\perp,j}$. Solenoidality again amounts to setting the divergence equal to zero, and gives a homogenous constraint that guarantees that all components of the third-order structure function are either zero or have the same scaling, but allows for scale-independent ratios between the components, similar to the second-order case. At higher orders than 3, there are no more solenoidality constraints, because structure functions contain terms such as $\langle z_{\perp,i}^{\pm}(0) z_{\perp,j}^{\pm}(0) z_{\perp,k}^{\pm}(\mathbf{r}_{\perp}) z_{\perp,l}^{\pm}(\mathbf{r}_{\perp}) \rangle$ whose divergence does not vanish (Lvov et al. 1997; Hill 2001).

Using the second-order structure function as an example, the longitudinal and transverse structure functions $S_{2,L}$, $S_{2,T}$ are not directly related to the conditional structure function $S_{2,3D}$ defined in Eq. (15). $S_{2,L}$ and $S_{2,T}$ are moments of the joint distribution $p(\delta z_{\perp}^{\pm}, \theta_{\delta z_{\perp}^{\pm}} | r_{\perp})$ of the field-increment amplitude δz_{\perp}^{\pm} and the angle $\theta_{\delta z_{\perp}^{\pm}}$, conditional on the separation distance r_{\perp} , viz.,

$$\begin{aligned} S_{2,L}(r_{\perp}) &= \int_0^{\infty} \int_0^{2\pi} (\delta z_{\perp}^{\pm})^2 \cos^2(\theta_{\delta z_{\perp}^{\pm}}) \\ &\quad \times p(\delta z_{\perp}^{\pm}, \theta_{\delta z_{\perp}^{\pm}} | r_{\perp}) d\delta z_{\perp}^{\pm} d\theta_{\delta z_{\perp}^{\pm}}, \\ S_{2,T}(r_{\perp}) &= \int_0^{\infty} \int_0^{2\pi} (\delta z_{\perp}^{\pm})^2 \sin^2(\theta_{\delta z_{\perp}^{\pm}}) \\ &\quad \times p(\delta z_{\perp}^{\pm}, \theta_{\delta z_{\perp}^{\pm}} | r_{\perp}) d\delta z_{\perp}^{\pm} d\theta_{\delta z_{\perp}^{\pm}}. \end{aligned} \quad (\text{A5})$$

We have shown that these functions must have the same scaling due to solenoidality. In contrast, the conditional structure function defined by Eq. (15) (ignoring for now the dependence on the third dimension via the angle $\theta_{B_{\text{loc}}}$) is the moment of the distribution of the field increment amplitude δz_{\perp}^{\pm} conditional on the angle $\theta_{\delta z_{\perp}^{\pm}}$ and the separation distance r_{\perp} :

$$S_{2,3D}(r_{\perp}, \theta_{\delta z_{\perp}^{\pm}}) = \int_0^{\infty} (\delta z_{\perp}^{\pm})^2 p(\delta z_{\perp}^{\pm} | \theta_{\delta z_{\perp}^{\pm}}, r_{\perp}) d\delta z_{\perp}^{\pm}. \quad (\text{A6})$$

Thus, in general, $S_{2,3D}$ coincides with neither $S_{2,L}$ at $\theta_{\delta z_{\perp}^{\pm}} = 0$

nor with $S_{2,T}$ at $\theta_{\delta z^\pm} = \pi/2$. Therefore, the scale-dependent anisotropy of the turbulence within the perpendicular plane as measured by $S_{2,3D}$ in Figure 1 cannot be expressed simply in terms of the solenoidality constraints.

REFERENCES

- Aitken A. C., 1936, *Proc. R. Soc. Edinburgh*, 55, 42
- Batchelor G. K., 1953, *The Theory of Homogeneous Turbulence*. Cambridge University Press
- Beresnyak A., 2014, *ApJ*, 784, L20
- Beresnyak A., 2015, *ApJ*, 801, L9
- Beresnyak A., Lazarian A., 2006, *ApJ*, 640, L175
- Boldyrev S., 2006, *Phys. Rev. Lett.*, 96, 115002
- Bruno R., Carbone V., 2013, *Living Rev. Solar Phys.*, 10, 2
- Chandran B. D. G., Schekochihin A. A., Mallet A., 2015, *ApJ*, 807, 39
- Chen C. H. K., Mallet A., Yousef T. A., Schekochihin A. A., Horbury T. S., 2011, *MNRAS*, 415, 3219
- Chen C. H. K., Mallet A., Schekochihin A. A., Horbury T. S., Wicks R. T., Bale S. D., 2012, *ApJ*, 758, 120
- Cho J., Vishniac E. T., 2000, *ApJ*, 539, 273
- Elsasser W. M., 1950, *Phys. Rev.*, 79, 183
- Goldreich P., Sridhar S., 1995, *ApJ*, 438, 763
- Goldreich P., Sridhar S., 1997, *ApJ*, 485, 680
- Grauer R., Krug J., Marliani C., 1994, *Phys. Lett. A*, 195, 335
- Greco A., Servidio S., Matthaeus W. H., Dmitruk P., 2010, *Planet. Space Sci.*, 58, 1895
- Hill R. J., 2001, *J. Fluid Mech.*, 434, 379
- Horbury T. S., Forman M., Oughton S., 2008, *Phys. Rev. Lett.*, 101, 175005
- Howes G. G., 2015, preprint, ([arXiv:1502.04109](https://arxiv.org/abs/1502.04109))
- Kadomtsev B. B., Pogutse O. P., 1974, *Soviet J. Exp. Theor. Phys.*, 38, 283
- Kolmogorov A., 1941, *Dokl. Akad. Nauk. SSSR*, 30, 301
- L'vov V. S., Podivilov E., Procaccia I., 1997, *Phys. Rev. Lett.*, 79, 2050
- Mallet A., Schekochihin A. A., Chandran B. D. G., 2015, *MNRAS*, 449, L77
- Maron J., Goldreich P., 2001, *ApJ*, 554, 1175
- Mason J., Cattaneo F., Boldyrev S., 2006, *Phys. Rev. Lett.*, 97, 255002
- Nazarenko S. V., Schekochihin A. A., 2011, *J. Fluid Mech.*, 677, 134
- Osman K. T., Kiyani K. H., Chapman S. C., Hnat B., 2014, *ApJ*, 783, L27
- Perez J. C., Chandran B. D. G., 2013, *ApJ*, 776, 124
- Perez J. C., Mason J., Boldyrev S., Cattaneo F., 2014, *ApJ*, 793, L13
- Podesta J. J., Chandran B. D. G., Bhattacharjee A., Roberts D. A., Goldstein M. L., 2009, *J. Geophys. Res.*, 114, 1107
- Politano H., Pouquet A., Sulem P. L., 1995, *Phys. Plasmas*, 2, 2931
- Schekochihin A. A., Cowley S. C., Dorland W., Hammett G. W., Howes G. G., Quataert E., Tatsuno T., 2009, *ApJS*, 182, 310
- Strauss H. R., 1976, *Phys. Fluids*, 19, 134
- Verdini A., Grappin R., 2015, *ApJ*, 808, L34
- Wicks R. T., Horbury T. S., Chen C. H. K., Schekochihin A. A., 2010, *MNRAS*, 407, L31
- Wicks R. T., Mallet A., Horbury T. S., Chen C. H. K., Schekochihin A. A., Mitchell J. J., 2013, *Phys. Rev. Lett.*, 110, 025003

This paper has been typeset from a \LaTeX file prepared by the author.